Real-Time Spectrum Analysis in Microstrip Technology

Miguel A. G. Laso, *Member, IEEE*, Txema Lopetegi, *Member, IEEE*, María J. Erro, *Associate Member, IEEE*, David Benito, María J. Garde, Miguel A. Muriel, *Senior Member, IEEE*, Mario Sorolla, *Senior Member, IEEE*, and Marco Guglielmi, *Senior Member, IEEE*

***Abstract*—We report on a time-domain analog in microwave lines to the spatial Fraunhofer (far-field) diffraction in paraxial conditions. Microstrip lines are used to design filtering configurations acting as spectrum analyzers. They are based on linearly chirped distributed Bragg coupling between the fundamental microstrip mode and the same but counterpropagating mode. Linearly chirped continuous impedance modulation in a microstrip line with varying upper plane strip-width will be shown to yield a mode-coupling location and group delay linearly distributed in frequency. Under the condition of a temporal equivalent to the spatial Fraunhofer inequality, the energy spectral density of the input signal is directly recoverable from the average output (reflected) power. It is only necessary to take into account a linear axis-change, given by the dispersion coefficient (group-delay slope) of the structure, from time to Fourier frequency. Both pulsed and nonpulsed RF signals are studied. Sequential time-gated segments of the input have to be processed in the nonpulsed case. The maximum frequency resolution achievable in this situation is discussed. The devices developed here could have important potential applications in the field of temporal signal processing, such as filtering using time-division techniques. Other application areas could be frequency-shift estimations using time-delay measurements in reflection, as well as the translation of path differences (temporal separation of signals) into frequency changes of an oscillatory interference pattern at the output.**

***Index Terms*—Characteristic impedance modulation, chirped Bragg coupling, dispersive delay line, Fourier-transform (FT) processors, microstrip technology, quadratic-phase filter.**

I. Introduction

THERE EXISTS in optics a well-studied mathematical duality between the equations that govern paraxial diffraction of beams in space and temporal narrow-band dispersion of pulses in dielectric media [1]. Both phenomena can be analyzed as parabolic differential equation problems (similar to diffusion problems with imaginary coefficients) resulting from some approximations to the wave equation. A monochromatic beam, initially confined transversally near the axis along which it propagates, is assumed in the spatial case. Monochromaticity leads to a delta function in the temporal-frequency spectrum and paraxial propagation to a narrow band of spatial frequencies around the origin of the spatial Fourier plane. Complementary assumptions are followed in the temporal case. Pulses, and hence a narrow band of temporal frequencies, are considered, and the spatial profile is ignored and approximated by a plane wave (i.e., monochromatic in the spatial–frequency spectrum). Kolner [1] revised the foundations of this space–time duality following Papoulis [2], and his works are a significant modern attempt toward a unified approach to both problems. The duality between paraxial spatial diffraction and temporal narrow-band (first-order) dispersion has led to fruitful transpositions of concepts from the space domain to the time domain (and vice versa).

Kolner and Nazarathy [4] extend the duality introducing the concept of *temporal lens*. A frequency chirp, i.e., a temporal quadratic phase shift imparted across an input pulse envelope, is analogous to the action of a thin spatial lens. A temporal lens modulates the phase of a temporal signal in the same way a spatial lens produces a phase modulation of the spatial field. Combining dispersive delay lines and chirp phase modulators that mimic free-space propagation and spatial lenses, respectively, temporal imaging systems were developed for distortionless stretching or compression of pulses for several applications [1], [5]–[7]. These systems consist of three subsystems in cascade: propagation in a dispersive line, transfer through a time lens, and again dispersive propagation in a delay line, in the same way that spatial imaging systems consist of a lens preceded and followed by free-space propagation.

Both paraxial diffraction and narrow-band dispersion can be analyzed as responses of all-pass quadratic-phase (linear group-delay) filters [2]. In [2], lenses are included for a common approach to spatial/temporal Fourier transform (FT) processors (that translate an input signal into a decomposition of its spatial/temporal spectral components), spatial/temporal signal compressors, and frequency filtering by spatial-windowing/time-gating. Related to the latter, a setup analogous to a spatial system of four focal lengths is proposed to filter an input signal by means of time gating, including in some applications phase modulation, in the joining of two FT processors. This way, convolvers and correlators can be implemented by an appropriate temporal processing of the output signal of an FT processor before the action of a second (inverse) FT processor [8]. Convolution and correlation theorems give freedom to calculate these operations as time-domain integrals or as multiplications in the frequency domain followed by (inverse) FTs (an FT and an inverse Fourier transform (IFT) represent

Manuscript received July 23, 2001; revised October 30, 2002. This work was supported by the Spanish Comisión Interministerial de Ciencia y Tecnología under Project TIC2001-2969-C03-03, Project TIC2001-3061, and Project TIC99-0292.

M. A. G. Laso, T. Lopetegi, M. J. Erro, D. Benito, M. J. Garde, and M. Sorolla are with the Electrical and Electronic Engineering Department, Public University of Navarre, E-31006 Pamplona, Spain (e-mail: mangel.gomez@unavarra.es).

M. A. Muriel is with the Telecommunication Engineering Department, Polytechnic University of Madrid, E-28040 Madrid, Spain.

M. Guglielmi is with the European Space Agency, European Space Research and Technology Center–European Space Agency, 2200 AG Noordwijk ZH, The Netherlands.

Digital Object Identifier 10.1109/TMTT.2003.808741

0018-9480/03$17.00 © 2003 IEEE

a mutually interdependent transform pair and a transform operation performed in isolation may be regarded as either the FT or the IFT).

This way, the original work of Papoulis on this space–time duality [2] provides new insight into pulse-compression techniques developed for instance in chirp radars [9] or optical fiber technology with chirp lasers [10]. Chirping and dispersive delaying can be viewed as a lens followed by diffraction focusing the aperture function (at the lens surface) to its FT (at the lens focal length). New understanding is also shed on the chirp-transformation techniques. These techniques decompose an FT operation into convolutions with chirped waveforms (i.e., transfers through diffractive/dispersive media) and multiplications with chirped waveforms (i.e., spatial/temporal phase modulations). They received serious interest after the appearance of high-performance surface acoustic wave (SAW) transversal filters acting as linear frequency-modulated filters [11].

In this paper, we present an example of this space–time duality in microstrip technology that requires only a high-dispersion and high-bandwidth stage similar to those reported previously [12]–[15]. The temporal action of this novel microstrip device is equivalent to the decomposition of a spatial aperture function into its FT components in the far-field Fraunhofer region in Fresnel conditions (paraxial diffraction). This way, the envelope of the output signal is the FT of the input envelope properly scaled to satisfy energy balance. It is worth noting that only the magnitude of the FT is recovered since the output is indeed phase-modulated by the phase terms of the device impulse response. There exist other arrangements, including not only dispersion but also time lenses, which could recover both magnitude and phase, but they are not the focus of the present work [2], [11].

The high-bandwidth and high-dispersive medium in microstrip can be implemented by a linearly chirped Bragg coupling between the quasi-TEM microstrip mode and the same but counterpropagating mode. This is achieved by varying continuously the impedance of the line either by altering the strip width or by etching the line ground plane. The continuous perturbation period is not constant like in [16]–[18], but it also changes linearly throughout the device length. Hence, the structure is locally tuned at a certain frequency within the operation bandwidth.

The paper is structured as follows. Section II is devoted to the derivation of the time domain analog to the spatial Fraunhofer diffraction. We will show that the output of a flat-amplitude and linear group-delay filter, whenever an analog to the spatial Fraunhofer condition is satisfied, is a phase-modulated signal whose envelope is proportional to the magnitude of the FT of the input envelope. The temporal axis is related to the Fourier frequency axis by the dispersion constant of the filter. Section III analyzes a simple design method for quadratic-phase filters in microstrip technology. In particular, we stress one approach to perform the linearly chirped continuous impedance modulation by means of a strip-width variation. The measured frequency response of a prototype following this technique is shown in Section IV to observe how well it fits to quasi-static analysis and full-wave electromagnetic simulation by commercially available software. The device is tested in Section V with different input signals to prove that it translates them into a temporal separation of their Fourier spectral components. For the case of nonpulsed signals, time-gated portions of the input are processed. This imposes a limit in frequency resolution, which is also discussed. Several potential applications for the real-time spectrum analysis in microstrip are envisaged. Some conclusions are pointed out in Section VI.

II. Theory: Time-Domain Analog to the Spatial Fraunhofer Diffraction

The chirp-transform algorithm splits any FT operation into three basic operations: premultiplication with a chirped waveform, convolution with a chirp filter (chirped impulse response), and postmultiplication with another chirped waveform. Moreover, the dual nature of convolution and multiplication in the time and frequency domains makes possible a convolution-multiplication-convolution arrangement that acts as an FT processor [11]. Convolution with a chirp filter is quadratic-phase filtering (diffraction/dispersion) [2] and multiplication with a chirped waveform is quadratic-phase modulation (spatial/temporal lens) [4]. This leads to the spatial classical diffraction-lens-diffraction scheme for an FT processor and its temporal dual dispersion-phase modulation-dispersion setup [2], [11]. Spatial/temporal FT processors differ from spatial/temporal imaging systems in the matching conditions between the frequency responses of their chirp-filtering subsystems and the phase modulation stage in the middle.

As a reduced version of this arrangement, if a signal is premultiplied with a chirped waveform and the result is convolved with a chirp filter, then the energy spectral density of the input signal is recoverable from the output signal [2], [11]. This is provided the delay versus frequency characteristic of the chirp filter is appropriately matched to that of the premultiplier chirp. This is the multiplication-convolution (lens-diffraction/dispersion) arrangement usually used for pulse compression [9], [10].

In this paper, we propose systems for real-time FT processing in magnitude, which do not require quadratic-phase modulation (lenses). The only requirement is an appropriate filtering configuration working as first-order dispersive medium. Its action is a time-domain equivalent to the Fraunhofer spatial diffraction in paraxial conditions, which decomposes an aperture into its spatial spectral components in the far field. In this section, we will show that, under certain assumptions, a high-bandwidth (enough to cover the signal bandwidth) and high-dispersion (linear group-delay of high slope) filter provides the required features to act as an analog to the Fraunhofer diffraction (Fig. 1).

Any linear time-invariant device is completely characterized by either its impulse response $h(t)$ or its transfer function $H(\omega)$, ω being the angular frequency, both related through the FT integral pair. A band-pass filter around ω_0 is said to be a quadratic-phase filter if the phase-term in the equivalent low-pass filter $H_{lp}(\omega')$ is, or can be approximated by, a second-order polynomial, i.e., if its Taylor series expansion around $\omega' = \omega - \omega_0 = 0$ can be truncated in the ω'^2 term

$$\varphi(\omega') \cong \varphi_0 + \omega' \cdot \dot{\varphi}_0 + \frac{1}{2!} \cdot \omega'^2 \cdot \ddot{\varphi}_0 \tag{1}$$

where $\varphi_0 = \varphi(\omega' = 0)$, $\dot{\varphi}_0 = \dot{\varphi}(\omega' = 0)$, and $\ddot{\varphi}_0 = \ddot{\varphi}(\omega' = 0)$.

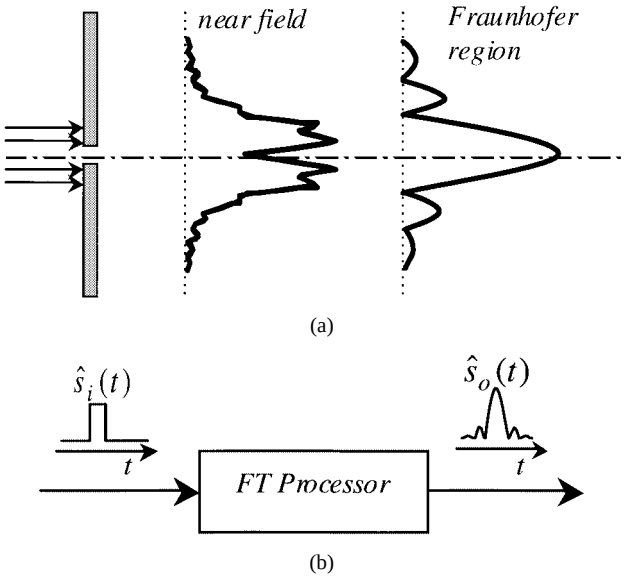

Fig. 1. (a) Spatial far-field Fraunhofer diffraction under paraxial conditions. (b) Time-domain analog for real-time spectral analysis.

Assuming frequency-independent insertion losses over the bandwidth where the filter phase is supposed to be quadratic, its impulse response can be obtained through the corresponding integral in the FT pair. Therefore,

$$h(t) \propto \cos\left(\omega_0 t + \frac{(t-\dot{\varphi}_0)^2}{2\ddot{\varphi}_0} + \text{constant}\right). \tag{2}$$

In (2), $h(t)$ is a chirped cosine waveform whose instantaneous angular frequency $\omega_i(t)$ is linearly distributed in time

$$\omega_i(t) = \omega_0 + \frac{t-\dot{\varphi}_0}{\ddot{\varphi}_0}. \tag{3}$$

The expression for the instantaneous frequency in (3) is simply the temporal ordering of frequencies imposed by the group delay of the quadratic-phase filter, which is linear with a slope $\ddot{\varphi}_0$.

Consider $s_i(t)$ as an input signal consisting of a carrier $\cos(\omega_0 t)$ which is modulated in amplitude by an information signal $\hat{s}_i(t)$. The output from the filter $s_o(t)$ is obtained by convolving the input signal with the impulse response given in (2). After several mathematical manipulations, we have

$$s_0(t) \propto \text{Re}\left(\text{FT}(\hat{s}_i(t))\big|_{\omega=(t-\dot{\varphi}_0)/\ddot{\varphi}_0} \cdot \exp\left(j\left(\omega_0 t + \frac{(t-\dot{\varphi}_0)^2}{2\ddot{\varphi}_0} + \text{constant}\right)\right)\right) \tag{4}$$

and hence

$$\hat{s}_0(t) \propto \left|\text{FT}(\hat{s}_i(t))\big|_{\omega=(t-\dot{\varphi}_0)/\ddot{\varphi}_0}\right|. \tag{5}$$

In the derivation of (4), $\hat{s}_i(t)$ was supposed to be confined to a small time width Δt_0 and the dispersion coefficient $\ddot{\varphi}_0$ was assumed to be large enough so that

$$\frac{\Delta t_0^2}{2\pi\left|\ddot{\varphi}_0\right|} \ll 1. \tag{6}$$

In (4) and (5), $\text{FT}(\hat{s}_i(t))\big|_{\omega=(t-\dot{\varphi}_0)/\ddot{\varphi}_0}$ is the FT of the input envelope $\hat{s}_i(t)$, evaluated at $\omega = (t-\dot{\varphi}_0)/\ddot{\varphi}_0$ for the time instant t. The incidence of a signal upon a flat-magnitude quadratic-phase band-pass filter does not affect the energy spectral density of this signal in the filter bandwidth $\Delta\omega$. However, the spectral components at the input belonging to $\Delta\omega$, are realigned in time (first-order dispersion makes different frequencies have a linearly distributed travel delay). Also, when the inequality in (6) is satisfied, there exists a single dominant frequency at a given instant of time. The amplitude spectrum of the input signal envelope is obtained following (5) over both negative and positive frequencies in the range from $-\Delta\omega/2$ to $\Delta\omega/2$. The inequality in (6) is a time-domain analog to the spatial Fraunhofer inequality $f \cdot \Delta x^2/(c_{\text{air}} \cdot d) \ll 1$ for an input spatial field confined to a circle of radius Δx, registering the diffracted image at a distance d, and c_{air} and f being the speed of light in air and the operation frequency, respectively. The output temporal axis is related to the Fourier frequency axis by the delay slope $\ddot{\varphi}_0$ through $\omega = (t-\dot{\varphi}_0)/\ddot{\varphi}_0$, where $\dot{\varphi}_0$ indicates the delay of the dc component of $\hat{s}_i(t)$. The maximum temporal width at the output is $\Delta t_{\max} = \Delta\omega \cdot |\ddot{\varphi}_0|$, since the bandwidth at the output is always constrained to $\Delta\omega$. This temporal width is the difference between the slowest and the fastest frequency in the filter bandwidth.

The presence of valid phase information for the FT of $\hat{s}_i(t)$ in the output signal can also be seen in (4). However, even demodulating the output signal with a frequency ω_0, the phase would be distorted by the quadratic temporal phase. Therefore, only the magnitude is directly recoverable following this scheme.

III. Quadratic-Phase Filters in Microstrip Technology: Discussion on the Design Process

In this section, the design of microstrip devices with a linear group delay of high slope over a wide frequency band in which insertion losses are approximately constant will be described. They will be used in Section V to perform the real-time energy spectral density analysis of signals, under the conditions discussed in Section II.

Let the characteristic impedance of a microstrip line be changed by a continuously changing profile. Consider, for example, a nonuniform microstrip line with a continuously varying strip width that follows a linearly frequency-modulated (chirped) continuous periodic function. Then, the phase-matching condition for resonant Bragg coupling between the quasi-TEM microstrip mode and the same but counterpropagating mode is ideally satisfied at only one position for each spectral frequency. This frequency will be reflected back from that position. In fact, if the perturbation is linearly chirped, then we will see that the location for mode coupling varies linearly in frequency and, as a result, the reflection time is a linear function of frequency also [19]. As the microstrip device works in reflective mode, it requires a directional coupler to retrieve the output signal at the input port. Linearly chirped Bragg coupling in reflection is well known in optical fiber grating technology (see [7] and references therein), mainly for the design of chromatic dispersion compensators in high-bit-rate and long-haul optical fiber links.

Consider $Z_0(z)$ as the modulated impedance given by

$$Z_0(z) = f_{\zeta(z)}(z) \tag{7}$$

where $\zeta(z)$ represents the modulation of the local spatial angular frequency of a continuous periodic function $f(z)$ and z is the

axis along which the microstrip line is extended from $z=-L/2$ to $z=L/2$, L being the device total length. It can be seen that if

$$\zeta(z)=\zeta_0+2\cdot C\cdot z \tag{8}$$

then $Z_0(z)$ yields a location for the coupling of modes that is linearly distributed in spectral frequency. In (8), the parameter $C(m^{-2})$ fixes the variation rate of the local spatial frequency and $\zeta_0=\zeta(z=0)$ is the value of the local spatial frequency at the device central point. The local spatial perturbation period $T(z)$ is derived from (8), and thus

$$T(z)=\frac{2\pi}{\zeta(z)}=\frac{2\pi}{\frac{2\pi}{a_0}+2Cz} \tag{9}$$

where $a_0=T(z=0)=2\pi/\zeta_0$ is the local spatial period at $z=0$, which fixes the central operation frequency ω_0.

The Bragg condition states that the perturbation period for an angular frequency ω to be coupled to the counterpropagating quasi-TEM mode in a microstrip line can be estimated as $\lambda_g/2$ (π-rad phase shift), λ_g being the guided wavelength at this frequency in the unperturbed (constant strip width) microstrip line [16]. Then, in the quasi-static (TEM) approximation, the angular frequency locally reflected at z, $\omega_l(z)$ is found as

$$\omega_l(z)=\frac{c}{2\cdot\sqrt{\varepsilon_{\text{eff}}|_{50\ \Omega}}}\cdot\left(\frac{2\pi}{a_0}+2Cz\right)\propto z \tag{10}$$

if an impedance modulation around 50 Ω is considered. In (10), $\varepsilon_{\text{eff}}|_{50\ \Omega}$ is the effective dielectric constant for a 50-Ω line in a low-frequency regime and c is the speed of light in vacuum. According to (10), a spatial frequency modulation like that in (8) provides a linear group delay in a bandwidth

$$\begin{aligned}\Delta\omega&=\left|\omega_l\left(z=\frac{L}{2}\right)-\omega_l\left(z=-\frac{L}{2}\right)\right|\\&=\frac{c}{\sqrt{\varepsilon_{\text{eff}}|_{50\ \Omega}}}\cdot|C|\cdot L\end{aligned} \tag{11}$$

around a central frequency

$$\omega_0=\frac{c\cdot\pi}{a_0\cdot\sqrt{\varepsilon_{\text{eff}}|_{50\ \Omega}}} \tag{12}$$

and with a delay slope

$$|\ddot{\varphi}_0|=\frac{2\sqrt{\varepsilon_{\text{eff}}|_{50\ \Omega}}}{c}\cdot\frac{L}{\Delta\omega}. \tag{13}$$

For negative (positive) values of C, higher (lower) frequencies are reflected first and the group-delay slope $\ddot{\varphi}_0$ is negative (positive).

Conversely, the design parameters C and L can be expressed as a function of $\ddot{\varphi}_0$ and $\Delta\omega$ through

$$L=\frac{c}{2\sqrt{\varepsilon_{\text{eff}}|_{50\ \Omega}}}\cdot|\ddot{\varphi}_0|\cdot\Delta\omega \tag{14}$$

$$C=2\cdot\left(\frac{\sqrt{\varepsilon_{\text{eff}}|_{50\ \Omega}}}{c}\right)^2\cdot\frac{1}{\ddot{\varphi}_0}. \tag{15}$$

If a low-pass signal $\hat{s}_i(t)$ with a time width Δt_0 is to be FT processed, then the microstrip spectrum analyzer must satisfy

$$\Delta\omega>\frac{2\pi}{\Delta t_0} \tag{16}$$

in order to provide an operation bandwidth wider than that of the signal as well as

$$L\gg\frac{c}{2\sqrt{\varepsilon_{\text{eff}}|_{50\ \Omega}}}\cdot\Delta t_0 \tag{17}$$

$$|C|\ll\pi\cdot\left(\frac{2\sqrt{\varepsilon_{\text{eff}}|_{50\ \Omega}}}{c\cdot\Delta t_0}\right)^2 \tag{18}$$

to fulfill the time-domain Fraunhofer inequality (6).

Although (10) roughly reduces the coupling position to a unique z value for each frequency, (10)–(18) still represent useful design expressions. Once the device length L and the variation rate of the local spatial frequency C in $f_{\zeta(z)}(z)$ have been fixed, the design can be checked in a straightforward way by obtaining its lossless behavior, which provides valid information on the approximated operation frequency range and delay characteristic. This is done by means of

$$\frac{dS_{11}}{dz}-2\cdot\gamma\cdot S_{11}-\frac{1}{2}\cdot\frac{d(\ln(Z_0))}{dz}\cdot\left(S_{11}^2-1\right)=0 \tag{19}$$

derived from the differential equations for voltage V and current I in a transmission line model [20]. In (19), the reflection coefficient S_{11} is solved for the input port $z=-L/2$. We take a purely imaginary propagation constant $\gamma=j\cdot\beta=j\cdot\sqrt{\varepsilon_{\text{eff}}}\cdot\omega/c$ (ε_{eff} depends only on the strip width in the quasi-static approximation). Equation (19) can readily be integrated numerically. At the endpoint, the reflection coefficient is supposed to be zero due to perfect matching for every frequency. This is taken as the final condition of the first-order nonlinear differential equation and the solution is integrated backward to obtain the reflection coefficient at the device input for any frequency.

The function $f(z)$ is chosen to minimize the frequency interference of the spurious reflected bands, at the harmonics of ω_0, in the main band since wide-band operation and nonrippled response are simultaneous requirements for an ideal FT processor. A nonchirped impedance modulation around 50 Ω with a spatial periodicity a_0 (for a central frequency of the device response around ω_0) such as $Z_0(z)=50\cdot\exp(\sin(z\cdot 2\pi/a_0))$ gives, through (19), a single-frequency-tuned response at ω_0. Any other choice of the periodic function would have led to frequency responses with reflected bands at $2\omega_0,\ 3\omega_0,\ldots$ This way, chirping will be applied to impedance modulations of the kind $\exp(\sin(z))$, since they seem suitable in this sense of suppression of the influence of the replicas. In terms of the coupled-mode theory [21], $-1/2\cdot d(\ln(Z_0))/dz$ in (19) is the coupling coefficient between the forward and backward TEM mode and, hence, such a variation of $Z_0(z)$ implies that the coupling coefficient is sinusoidal. Anyway, the replicas will be also constrained to reduced levels as long as $f(z)$ is continuous and smooth.

The same idea of continuous and smooth impedance modulation has been used to significantly reduce the level of the rejected bands at the harmonics of the design frequency in a microstrip band reflector with patterns etched in the ground plane [17], [18].

This way, the impedance modulation finally implemented is

$$Z_0(z) = 50 \cdot \exp\left(A \cdot W(z) \cdot \sin\left(\frac{2\pi}{a_0} \cdot z + C \cdot z^2 - C \cdot \left(\frac{L}{2} \right)^2 \right) \right) \tag{20}$$

where the phase of the sine wave is simply the integral of the local spatial frequency $\zeta(z)$. In (20), A is a weight factor of the impedance modulation and $-C \cdot (L/2)^2$ is the integration constant fixed at this value to have input and output ports of 50 Ω, whenever L is a multiple of a_0. Smoother input and output impedance transitions are achieved if a windowing function $W(z)$ is used. Reflections from the extremes of the structure give rise to different long-path Fabry–Perot like resonances, which cause undesirable rapid ripple to appear around the mean values in the magnitude and group-delay versus frequency patterns. This degrades the FT processor performance. The maximum amplitude (peak to peak) of these oscillations can be reduced using tapering techniques, proposed, for example, in [22] for microstrip reflectors with ground plane etching. These tapering techniques diminish the impedance perturbation smoothly toward the device endpoints. If the bandwidth of the processed pulse is larger than the spacing between the oscillations, which is a common case for these long wide-band devices, then this rapid and small ripple becomes less important and only the mean value is relevant.

On the other hand, the attenuation due to dielectric and conductor losses, in units of Nepers per meter (Np/m), increases with ω and $\sqrt{\omega}$, respectively (see, for example, [23]). Negative values of C imply higher (high-loss) frequencies reflecting earlier in the transmission line. This gives a behavior better equalized than with positive C's. However, for most microstrip substrates, conductor loss is much more significant than dielectric loss. Hence, attenuation could not be still conveniently equalized in the operation bandwidth even with a linearly distributed location for mode coupling. Then, $W(z)$ is made asymmetric to favor the longer lossy round trips of lower frequencies reflected at the device terminal end. This way, the perturbation is stronger for those z values corresponding to the lower frequency band $(z > 0)$.

We next present an example of implementation of the time-domain Fraunhofer approximation. In particular, we design microstrip devices with a linearly chirped location for mode coupling, which allows them to work as Fourier transformers of signals with time widths Δt_0 around 0.6 ns. For a 50-mil-thick substrate with relative dielectric constant $\varepsilon_r = 10.2$, the effective dielectric constant for a 50-Ω-microstrip line at quasi-TEM analysis is $\varepsilon_{\text{eff}}|_{50\ \Omega} \cong 6.8$, and the central spatial perturbation period a_0 for a central operation frequency around 9 GHz is 6.4 mm. The Fraunhofer condition is satisfied when the device length L is much greater than 3.5 cm, and, simultaneously, the chirp parameter C verifies that $|C|$ is much smaller than 2600 m^{-2} approximately, making use of (17) and (18), respectively. Then, the device bandwidth can be obtained through (11) to give $\Delta\omega \cong 10$ GHz $\cdot$ rad, covering barely the signal bandwidth, which is roughly estimated as $\approx 2\pi/\Delta t_0$. It must be noted, moreover, that this theoretical bandwidth diminishes because of the impedance windowing. Equation (11) suggests two different ways to increase the bandwidth: increase $|C|$, which is incompatible with the Fraunhofer condition or, alternatively, increase L. We will fix L to be $50 \cdot a_0$. The chirp parameter C must be negative for flat equalized frequency response. The upper limit for $|C|$ is fixed by the Fraunhofer condition in (18), and the lower one fixed by the operation bandwidth in (11). In this example, a C–value set to $-2080\ \text{m}^{-2}$ will be shown to be adequate. The profile of $W(z)$ is asymmetric, as required, and Gaussian

$$W(z) = \exp\left(-4 \cdot \left(\frac{z - \frac{L}{4}}{L} \right)^2 \right). \tag{21}$$

Any other choice would be possible, but the Gaussian window is widely employed in several other applications both in optics and microwave technology. Finally, the amplitude factor of the impedance modulation A is set to 0.4.

Once all the parameters in (20) have been fixed, we implement the impedance variation as a strip-width modulation [23]. As the impedance varies between 35 and 75 Ω, the strip width changes between 0.5 and 2.5 mm approximately. In Fig. 2, the S_{11} parameters obtained through (19) in a lossless and quasi-static approximation (thin solid line) and through the commercially available full-wave electromagnetic simulator Agilent Momentum (thick solid line) are compared. The device provides the required features between 3 and 14 GHz approximately, with a delay slope, calculated over the graph, $\ddot{\varphi}_0 \cong -83\,000\ \text{ps}^2/\text{rad}$. The commercial simulator estimates a nearly flat -3-dB reflected band (dielectric loss tangent $\tan\delta = 0.0026$ and metal conductivity $\sigma = 5.8 \cdot 10^7$ S/m). When perfectly matched terminations at $z = \pm L/2$ are supposed, as it is automatically done in the solution of (19) (thin solid line) for any frequency, no significant ripple can be seen either in the magnitude or in the group delay of the reflection coefficient if tapering is used (Fabry–Perot-like resonances are almost eliminated). Actually, the whole strip pattern has slight microstrip mode dispersion. This causes a more realistic ripple to appear in the full-wave simulation (thick solid line) even with ideal 50-Ω connectors at the input and output ports. However, this ripple is fast and small enough to be neglected in practical applications.

The average internal power distribution can be calculated as a function of the position in the device by obtaining $|A^+(z)|^2 + |A^-(z)|^2$ for every frequency, $A^{\pm}$ being the complex amplitudes of the forward $(+)$ and backward $(-)$ quasi-TEM mode. These values are related to the voltage and current along the transmission-line model, $V = \sqrt{Z_0} \cdot (A^+ + A^-)$ and $I = (A^+ - A^-)/\sqrt{Z_0}$ [24], so that the differential equations for voltage and current lead to

$$\left.\begin{aligned} \frac{dA^+(z)}{dz} &= -\gamma \cdot A^+(z) - \tfrac{1}{2} \cdot \frac{d(\ln(Z_0(z)))}{dz} \cdot A^-(z) \\ \frac{dA^-(z)}{dz} &= -\tfrac{1}{2} \cdot \frac{d(\ln(Z_0(z)))}{dz} \cdot A^+(z) + \gamma \cdot A^-(z) \end{aligned}\right\}. \tag{22}$$

In fact, the Riccati equation in (19) is obtained from (22) by taking into account that the reflection coefficient is $S_{11} = A^-/A^+$.

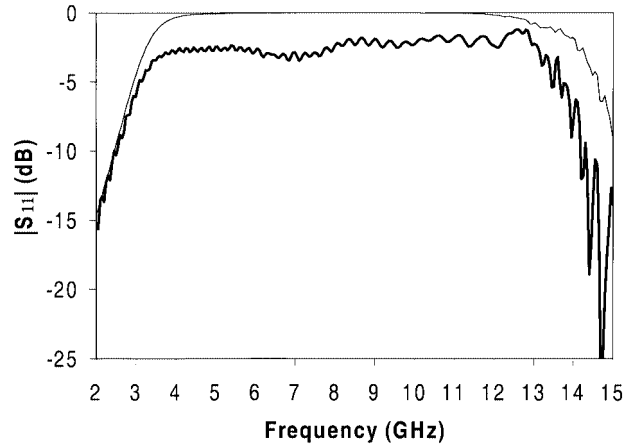

(a)

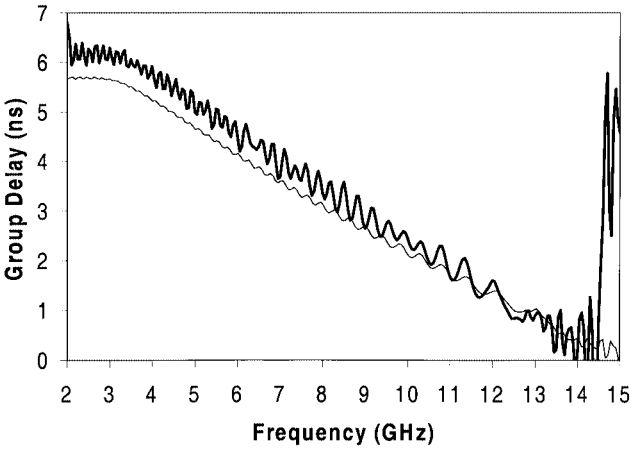

(b)

Fig. 2. S_{11}-parameter of the microstrip quadratic-phase filter (a) magnitude and (b) group delay obtained through the lossless quasi-static approximation (thin solid line) and through a full-wave electromagnetic simulation (thick solid line).

Fig. 3 shows the system average internal power distribution in the operation bandwidth, as relative brightness levels, solving (22) for $A^{+}(z)$ and $A^{-}(z)$ in the quasi-static approximation. This two-dimensional (2-D) distribution relates the group delay (on the left of the figure) with the perturbation period in the strip pattern (at the top). A location for mode coupling linearly distributed in frequency is clearly observed as well as the higher frequencies being reflected back earlier than the lower ones (negative C).

This device translates an input signal of time width around 0.6 ns into a temporal separation of its spectral components following the group delay versus frequency characteristic. The minimum pulse duration for an adequate performance of the FT processor will be fixed by the filter bandwidth, say $\Delta t_{0,\min} \cong 4\pi/\Delta\omega$, and the maximum fixed by the dispersion coefficient through the Fraunhofer inequality. However, these minimum and maximum time widths should be considered only as reference values. Even when signals with the same time width are supposed, their spectra might be very different, and the FT processor could order in time the spectral components more easily for some signals than for others. Hence, the actual tuning range for the input time width depends largely on the type of incident signal. Often, satisfactory results are obtained even when the

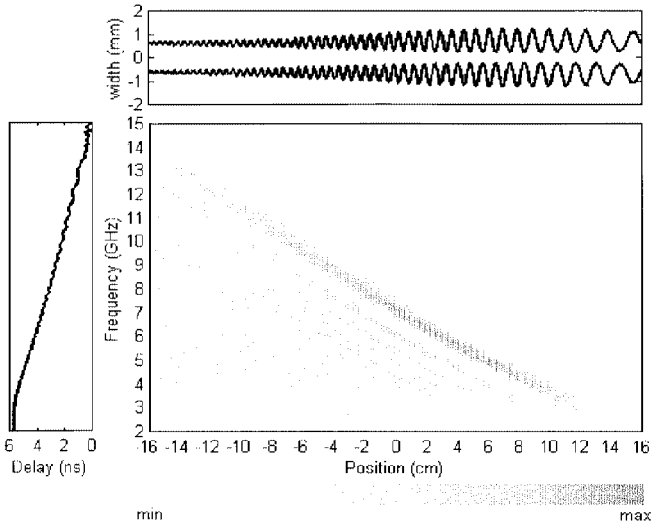

Fig. 3. Average internal power as a function of frequency and position in the microstrip quadratic-phase filter using the transmission-line model. Top: strip pattern (not to scale). Left: group-delay.

Fraunhofer condition is relaxed, so that the reference value for the maximum time width is $\Delta t_{0,\max} \cong \sqrt{2\pi\,|\ddot{\varphi}_0|}$. The input signal can be a pulse sequence. In this case, the group-delay slope must be sufficiently large to guarantee that the Fraunhofer condition for spectral ordering is fulfilled for the duration of the whole sequence. Additionally, the processor bandwidth should be at least as broad as the spectrum of each individual constituent of the sequence. For nonpulsed signals, time-gated segments of the input have to be processed as consecutive pulses. This time gating introduces a limit in frequency resolution that will be studied in Section V.

The exact fields of a microstrip line constitute a hybrid TM–TE wave. However, for most practical applications, the dielectric substrate is electrically very thin, and so the fields are approximately the same as for the static (TEM) case. A negative value of C appears again as an optimum choice since mode-dispersion effects are minimized when high dispersive frequencies are reflected earlier in the structure. This way, even with wide bandwidths, the quasi-static approximation and the dispersive analysis lead to similar results in our case. If necessary, though, this quasi-static approach could be the first step toward the ultimate design, accounting for mode dispersion later so that the frequency dependence of the effective dielectric constant [25] is also considered in the Bragg condition of (10).

With respect to parasitic effects in microstrip (radiation losses and surface-wave propagation), they are maintained within negligible values due to the smooth strip shape. Other undesirable effects like strong coupling between the quasi-TEM mode and the lowest order TM mode or excitation of transverse resonant modes in the widest strip locations, which can also couple strongly to the quasi-TEM mode, could restrict the maximum operation frequency (see [26] and references therein). The designer should check that the device works safely below that maximum frequency.

We have also tested satisfactorily another microstrip changing profile for impedance modulation. Slots of varying width etched in the ground plane, parallel to the upper conductor strip, modify the impedance and propagation constant

seen by the wave traveling along the line. Finite-difference time-domain (FDTD) numerical simulations [27] could be performed to obtain the dependence of both the characteristic impedance and the effective dielectric constant with respect to the slot width. Microwave researchers have taken a special interest over the last few years in microstrip ground plane etching techniques because of their potential capabilities to implement photonic bandgap (PBG) structures [17], [18], [22], [27], [28], recently pointed out as promising ways to design rejection filters in future mobile communication terminals and related fields (see [26, pp. 384–385]).

Finally, although microstrip has been chosen in this paper, the same ideas are applicable in stripline, coupled stripline, or coplanar structures. Dispersive delay lines in SAW technology are well known since the early 1970s [29], [30]. In contrast to the continuous impedance modulation described above for a microwave transmission line, SAW devices have only one impedance step over a distance equal to half a wavelength. This seriously limits the maximum fractional bandwidth achievable with SAW devices due to the presence of harmonic responses, whereas it is easily greater than 100% in our case. Moreover, nowadays the frequency range for SAW technology is only up to 3 GHz [31] and the reported insertion losses of dispersive delay lines have been usually greater than 25 dBs [32].

Some other authors have tried to obtain the dispersive behavior of SAW delay lines in microwave transmission lines [33]–[35]. They have used a numerical method originally developed for the synthesis of SAW devices fitting a specified response [36]. The approach described here is much simpler. Likewise, it is more confined to the topic in hand and it provides much further insight into the device operation.

IV. Measurements

The prototype designed in Section III was constructed by means of a numerical milling machine on a Rogers RO3010 substrate 50 mil thick, with relative dielectric constant $\varepsilon_r = 10.2$, dielectric loss tangent $\tan\delta = 0.0026$, and metal conductivity $\sigma = 5.8 \cdot 10^7$ S/m. If the device impulse response were calculated by means of the IFT of its frequency response measured in reflection, it would show the dependence of the Bragg resonant frequency with the position along the axis of the microstrip line (the higher frequencies would appear at the beginning and the lower ones at the end of the signal). As the impulse propagates through the system, each segment that it interacts with is slightly different due to the changing perturbation period. Thus, the frequencies that are reflected vary and, if an adequate design is done for equalized losses across the operation frequency range, then the overall reflected pulse has a square-like shape with sharp rise and fall times. The total duration of the reflected impulse response is equal to the round-trip propagation time through the device. In the intended solution as integrated circuit, both the input and output sections of the prototype will also be microstrip lines and the mismatch effects of the real SMA connectors will be automatically overcome. Then, we use an appropriate time gating to isolate the impulse response from the reflection peak that appears when the impulse just encounters the input connector, and from an oscillatory tail because of the end-to-end resonance.

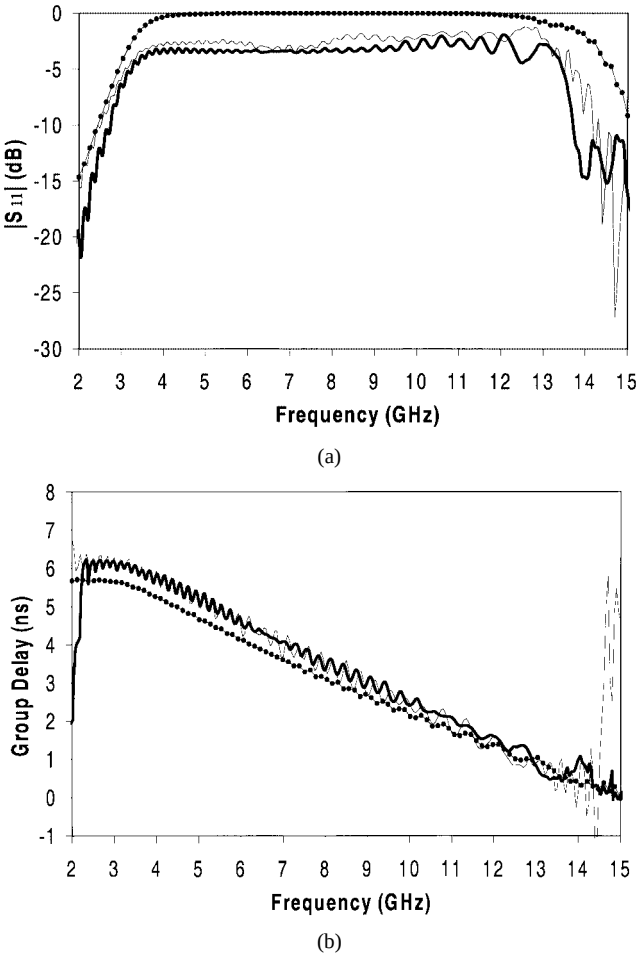

Fig. 4. S_{11}-parameter of the microstrip quadratic-phase filter (a) magnitude and (b) group delay obtained through the lossless quasi-static approximation (dotted line), commercial software (thin solid line), and measurement (thick solid line).

This way, in Fig. 4, the S_{11} parameter of the measurement (directional coupler not included), after time processing (thick solid line), is compared in magnitude a and group delay b with the lossless and quasi-static approximation (now in dotted line) and with the commercial full-wave electromagnetic simulation (now in thin solid line). The measurement in Fig. 4 shows that the prototype truly provides the required features of flat magnitude and linear group delay.

V. Examples of Energy Spectral Density Analysis

By means of several examples, the device designed in Section III will be shown here to make the input spectral components undergo a strong temporal ordering process following the linear dispersion characteristic of the microstrip quadratic-phase filter. As a result, the shape of the system output (reflected) signal envelope $\hat{s}_0(t)$ matches the FT magnitude of the input signal envelope $\hat{s}_i(t)$ over a bandwidth as broad as that of the device. As discussed in Section II, the angular Fourier frequency axis ω and the output temporal axis t are related by the dispersion coefficient (delay slope) of the structure $\ddot{\varphi}_0$, following the group-delay curve.

The device with varying strip width designed in Section III was conceived to act as a Fourier transfomer of pulses of width

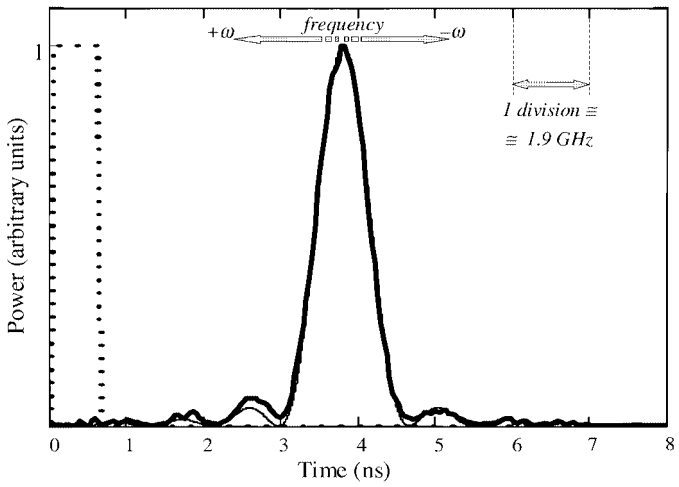

Fig. 5. Simulation of the real-time FT processor. The average power of the input pulse (dotted line), an ideal rectangular pulse 0.6-ns wide, is depicted together with the average output power reflected from the device (thick solid line). Signals are normalized to their maximum power. The thin solid line is the squared theoretical FT magnitude (energy spectral density) of the input signal over a temporal axis related to the frequency axis by $\ddot{\varphi}_0$.

around 0.6 ns. We assume the signals to be centered at the system central frequency, $\omega_0 = 2\pi \cdot 8$ GHz $\cdot$ rad. We obtain the reflected signal spectrum by multiplying the measured frequency response of the device and the input signal spectrum. The corresponding output time waveform is then recovered by taking the IFT.

The first example deals with a 0.6-ns-width ideal rectangular pulse. In Fig. 5, the average power of the input pulse (dotted line), $\hat{s}_i^2(t)$, at the left on the graph, is represented together with the average output power reflected from the device (thick solid line), $\hat{s}_o^2(t)$ and the squared theoretical FT-magnitude (energy spectral density) of the input (thin solid line; in this last case over a temporal axis related to the frequency axis by $\ddot{\varphi}_0$). To make the device behavior clearer, we represent all signals normalized to their maximum power. It is observed that, when the temporal Fraunhofer condition is fulfilled, this guarantees a temporal ordering of the spectral components strong enough so that only a single dominant frequency component exists at each time instant. Thus, the shape of the FT magnitude of the input signal envelope is closely reproduced. The differences between the theoretical energy spectral density of the input pulse and that predicted by the real FT processor (thin and thick solid lines, respectively, in Fig. 5), are explained by the weak distortion suffered by the signal due to the ripple in the device measured reflectivity characteristic (Fig. 4). The output signal envelope has a time width between the two first minimum-power points of ≈ 1.7 ns. This implies a spectral width of ≈ 3.25 GHz ($|\ddot{\varphi}_0| = 83\,000$ ps^2/rad. This is in close agreement with the bandwidth of the main lobe of the ideal sinc function when Fourier transformation is applied to a 0.6-ns-wide rectangular pulse $(2/0.6 \text{ ns} \cong 3.3 \text{ GHz})$.

This effect of temporal separation of spectral components can be employed, for example, to filter out undesirable frequencies by using time-division techniques. Low-, band-, or high-pass filtering needs only time gating (the filter center frequency being set by the gate timing and the filter bandwidth by the gate duration and shape) in the joining between two identical FT processors but with opposite delay slopes. The requirements for the temporal gate to control the filter selectivity (gate rise and fall times) can be partially alleviated by the dispersion of the microstrip filter, since the output signal can be stretched using higher delay slopes.

If the signal does not satisfy the Fraunhofer condition, then the reflected average power would not match the energy spectral density of the input. In this case, the dispersion would not be high enough to get an effective temporal separation of the input spectral components, and so the output pattern would reproduce that of the spatial Fresnel (near-field) diffraction [38].

The system performance for pulse sequences is also evaluated. This time, the Fraunhofer condition should be guaranteed for the whole sequence duration as well as the device bandwidth should be, at least, as broad as the frequency width of the narrowest temporal constituent of the sequence. In Figs. 6 and 7, we use sequences composed of Gaussian pulses like $\hat{s}_i^x(t) = \exp(-1/2 \cdot (t/\Delta\tau)^2)$, where $2\sqrt{\ln 2} \cdot \Delta\tau$ is the temporal full-width at half-maximum (FWHM). In Figs. 6 and 7, $\Delta\tau$ is fixed at 50 ps. Fig. 6 shows a two-Gaussian-pulse signal with three different sequence durations (the sequence total time width is defined as the distance between the first and the last pulse in the sequence): $\Delta t_0 = 0.6$ ns in Fig. 6(a), $\Delta t_0 = 1$ ns in Fig. 6(b), and $\Delta t_0 = 0.3$ ns in Fig. 6(c). The input sequence (given in average power by the dotted line) is depicted together with the system average output power (thick solid line), which fits the theoretical energy spectral density of the input signal (thin solid line). An interference pattern can be seen, which is modulated in amplitude by the energy spectral density of a single Gaussian pulse (dashed line). This interference pattern resembles that of the Young experiment on double-slit far-field spatial diffraction (actually, the same phenomenon can be generalized to sequences composed of N pulses and spatial diffraction gratings of N slits) [38]. In fact, the frequency of the oscillatory interference pattern can be shown to be a function of the whole sequence duration by simply obtaining the theoretical FT of the input

$$\hat{s}_0(t) \propto \Delta\tau \cdot \sqrt{2\pi} \cdot \left| \frac{\sin\left(2 \cdot \frac{t-\dot{\varphi}_0}{\ddot{\varphi}_0} \cdot \frac{\Delta t_0}{2}\right)}{\sin\left(\frac{t-\dot{\varphi}_0}{\ddot{\varphi}_0} \cdot \frac{\Delta t_0}{2}\right)} \right| \cdot e^{-(1/2)\cdot((t-\dot{\varphi}_0)/\ddot{\varphi}_0 \cdot \Delta\tau)^2}. \quad (23)$$

The last exponential factor in (23) is the FT of a Gaussian pulse modulating the $|\sin(2x)/\sin(x)|$-like interference term. The frequency of this interference is $\Delta t_0/2\pi\,|\ddot{\varphi}_0|$. Then, as the sequence time width increases [Fig. 6(b)], the interference frequency also increases. On the contrary, as the Gaussian pulses are closer together, the interference is of lower frequency [Fig. 6(c)]. This could be used to measure temporal separations, for example, between a signal and a delayed version of it, as frequency changes in the output signal.

A deep insight into the system behavior can be obtained by representing the signals in both time and frequency domains simultaneously. The larger plots of Fig. 7 show the joint time–frequency energy distributions (a) for the two-Gaussian-pulse

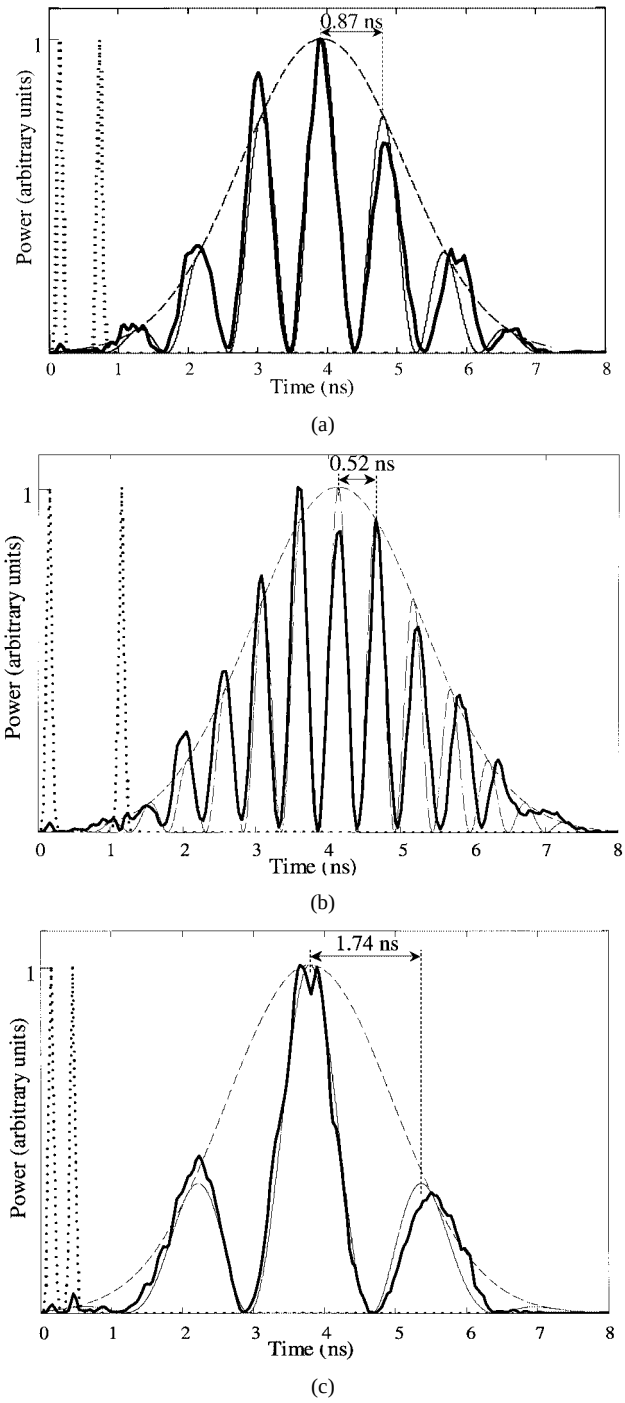

Fig. 6. Simulation of the real-time FT processor. The average power of the input sequence (dotted line), a two-Gaussian-pulse train with $\Delta\tau = 50$ ps, is depicted together with the average output power reflected from the device (thick solid line) when the sequence time width is (a) $\Delta t_0 = 0.6$ ns, (b) $\Delta t_0 = 1$ ns, and (c) $\Delta t_0 = 0.3$ ns. Signals are normalized to their maximum power. The thin solid line and the dashed line are the theoretical energy spectral densities of the input sequence and of a single Gaussian pulse, respectively, over a temporal axis related to the frequency axis by $\ddot{\varphi}_0$.

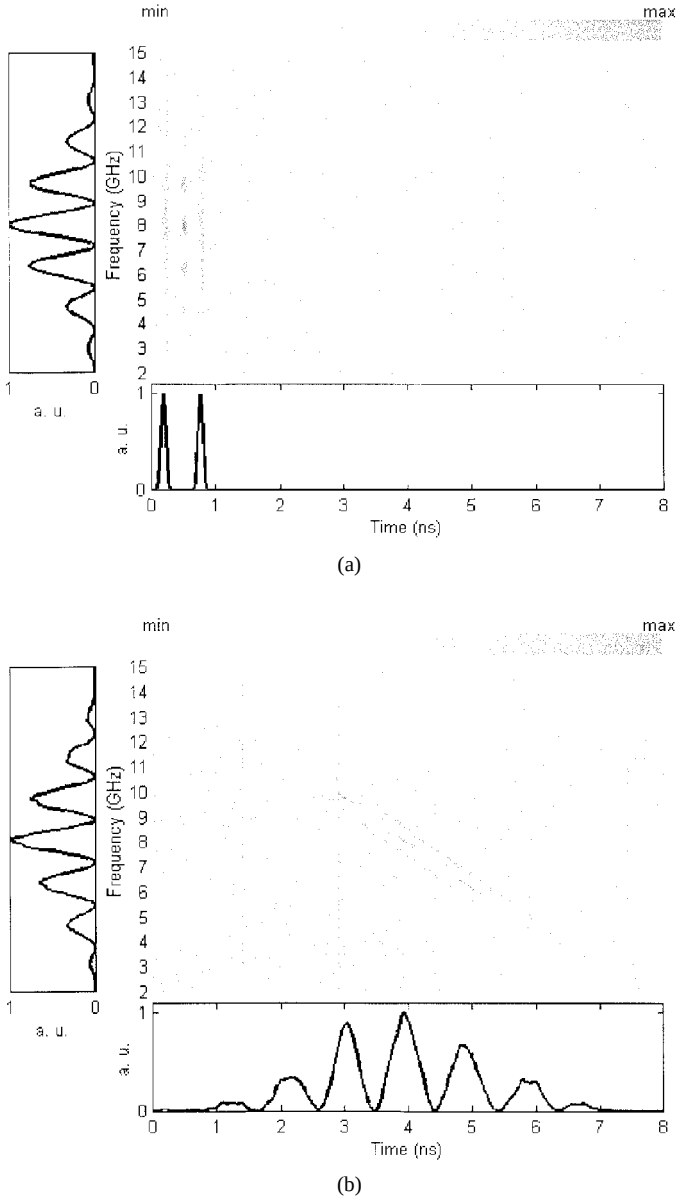

Fig. 7. Simulation of the real-time FT processor by using joint time–frequency representations. (a) Input signal: the normalized average power of the signal, a two-Gaussian-pulse train with $\Delta\tau = 50$ ps and sequence width $\Delta t_0 = 0.6$ ns, is depicted at the bottom. The plot on the upper left shows the normalized energy spectral density of the signal in the frequency domain. The larger plot shows the joint time-frequency representation of the signal by using the Wigner-Ville distribution. (b) Output signal with the same definitions as for (a).

train considered in Fig. 6(a) with $\Delta\tau = 50$ ps and sequence duration $\Delta t_0 = 0.6$ ns and (b) for the corresponding system output as relative brightness levels (in this case using a Wigner–Ville distribution [39], [40]). This kind of representation provides information about the temporal location for each spectral component. In Fig. 7(a) and (b), the input and output signals, respectively, are also represented separately in the time domain (at the bottom), as normalized average power signals, and in the frequency domain (on the upper left) as normalized energy spectral densities. It is observed that the output signal retains spectral components identical to those of the incident signal (except for the weak distortion due to the ripple in the system frequency characteristic). However, these components suffer a strong process of linear ordering in time according to the linear group delay of the system.

The above analysis of pulsed RF signals is now extended to nonpulsed inputs. In this case, sequential time-gated portions of the input must be processed. The maximum repetition rate

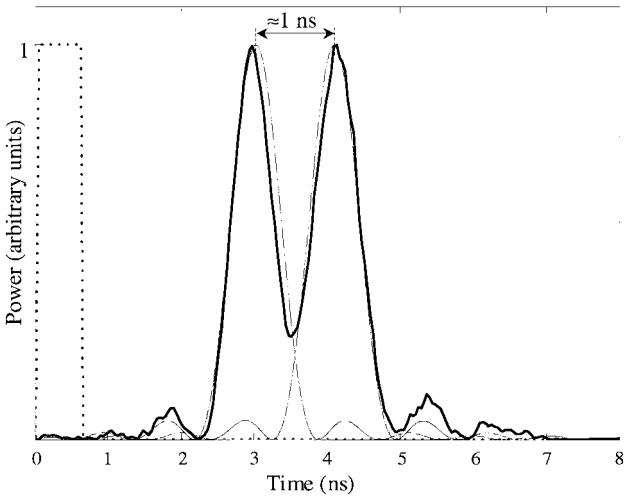

Fig. 8. Simulation of the real-time FT processor. The average power of the input pulse (dotted line), a double-carrier rectangular pulse 0.6-ns wide (which is actually a fragment of a time-gated stationary signal consisting of two sine waves), is depicted together with the average output power reflected from the device (thick solid line). Signals are normalized to their maximum power. The thin solid lines are the theoretical energy spectral densities of two single-carrier 0.6-ns-wide rectangular pulses at $\omega_{0,1} = 2\pi \cdot 7.5$ GHz $\cdot$ rad and $\omega_{0,2} = 2\pi \cdot 9.5$ GHz $\cdot$ rad, respectively, over a temporal axis related to the frequency axis by $\ddot{\varphi}_0$.

of this processing window is imposed by the maximum temporal width at the output, which was discussed in Section II. A stationary signal consisting of two sine waves ($\omega_{0,1} = 2\pi \cdot 7.5$ GHz $\cdot$ rad and $\omega_{0,2} = 2\pi \cdot 9.5$ GHz $\cdot$ rad) is considered in Fig. 8. The signal is divided into consecutive 0.6-ns-wide fragments in order to be analyzed in spectral components. The problem is then reduced to the analysis of rectangular pulses like the one considered in Fig. 5, but now modulating two carrier frequencies simultaneously. The average reflected power (thick solid line) is compared to the theoretical energy spectral densities (thin solid lines) of two single-carrier 0.6-ns-wide rectangular pulses at $\omega_{0,1}$ and $\omega_{0,2}$, respectively. Two sinc functions can be seen interfering with a time separation around 1 ns. This agrees with the $\omega_{0,2} - \omega_{0,1} = 2\pi \cdot 2$ GHz $\cdot$ rad spectral separation of the carriers. This way, the identification of distinct harmonics as well as the frequency shift between them are translated into estimations of time delays. The measurement of these temporal separations could be done on an easily accessible time scale if high delay-slope devices are designed.

For the case of nonpulsed stationary signals, the global output consists of the output for a single fragment of the time-gated signal being repeated in time indefinitely. For nonpulsed nonstationary signals, the analysis also shows the evolution of the spectral components with time.

Time gating imposes a limit in frequency resolution on nonpulsed signals. If T is the time gate duration, then we take $\Delta f_r = 1/T$ as the minimum resolvable frequency distance. The longer the time gate duration, the better the frequency resolution. However, the maximum value of T is also fixed by the Fraunhofer inequality. This means a minimum separation around $\Delta f_r \cong \sqrt{1/(2\pi|\ddot{\varphi}_0|)}$ for two frequencies to be resolved. This way, the maximum resolution can be estimated as the square root of the ratio of the device bandwidth to the total delay variation within this bandwidth. To increase the resolution, the relative delay can be increased, while the operation bandwidth remains fixed, either by making the device longer, benefiting from the feasibility to coil/meander the structure [41], or by forcing the wave to travel slower (using, for instance, high dielectric constant substrates).

VI. Conclusion

In this paper, we have reported on a time-domain analog to the spatial Fraunhofer (far-field) diffraction in Fresnel conditions. It consists of a microstrip line with chirped distributed resonant Bragg coupling in reflection between the fundamental microstrip mode and the same but counterpropagating mode. This idea was useful in the design of filtering configurations acting as spectral analyzers.

We have presented a unified approach to the design of broad-band and high-dispersive quadratic-phase (linear group-delay) microstrip filters. They are based on a continuously changing line profile and are the analogs, in this space–time duality context, to free-space propagation. Linearly chirped continuous impedance modulation in a microstrip line with varying upper plane strip width (a varying ground plane slot profile would be also valid) has been proved to yield both a location for mode coupling and a group delay linearly distributed in frequency. Then, the input spectral components undergo a temporal ordering process following the linear dispersion characteristic of the quadratic-phase filter. Under the condition of a temporal equivalent to the spatial Fraunhofer inequality, which implies a dispersion high enough in the input signal bandwidth, the shape of the system output (reflected) signal envelope coincides with the FT magnitude of the input signal envelope over a bandwidth as broad as that of the device. Therefore, the energy spectral density of the input signal is directly recoverable from the output average power by simply taking into account a linear axis change given by the dispersion coefficient (group-delay slope) of the structure. The full theoretical background for this derivation has been described in Section II and the design methodology in Section III.

In Section V, we have tested our designs by simulating the system response to different theoretical input signals using the reflectivity characteristics measured in Section IV. Both single pulses and sequences were considered. Nonpulsed signals were also studied and the frequency resolution was addressed. Interesting applications in the field of temporal signal processing, such as filtering using time-division techniques, have been pointed out. Frequency-shift estimations using time-delay measurements in reflection, as well as the translation of temporal separations (path differences) into frequency changes in the oscillatory term at the output, could have further potential applications.

This device has been developed as part of a well-established space–time duality between paraxial spatial diffraction and temporal signal dispersion. Both physical phenomena can be modeled by quadratic-phase filters, shedding new light and

understanding into previous knowledge as the chirp-transform algorithm and radar pulse compression techniques broadly known among microwave researchers. New devices in microstrip technology can be advanced, owing to this analogy and the quadratic-phase filters proposed here, and opening important new perspectives in the mentioned scientific fields. Programmable convolvers/correlators, variable delay lines, and magnitude and phase Fourier spectral analyzers (as components of network and spectrum analyzers) are a few of them.

ACKNOWLEDGMENT

The authors would like to thank J. Capmany, Polytechnic University of Valencia,Valencia, Spain, for helping with the measurements of the prototypes. Many thanks also to T. Närhi, European Space Agency, ESTEC-ESA, TOS-ETP, Noordwijk, The Netherlands, for his comments about this paper.

REFERENCES

[1] B. H. Kolner, "Space-time duality and the theory of temporal imaging," *IEEE J. Quantum Electron*, vol. 30, pp. 1951–1963, Aug. 1994.

[2] A. Papoulis, *Systems and Transforms With Applications in Optics*. New York: McGraw-Hill, 1968.

[3] ——, "Pulse compression, fiber communications, and diffraction: A unified approach," *J. Opt. Soc. Amer. A, Opt. Image Sci.*, vol. 11, no. 1, pp. 3–13, Jan. 1994.

[4] B. H. Kolner and M. Nazarathy, "Temporal imaging with a time lens," *Opt. Lett.*, vol. 14, no. 12, pp. 630–632, June 1989.

[5] ——, "Temporal imaging with a time lens, erratum," *Opt. Lett.*, vol. 15, no. 11, p. 655, June 1990.

[6] A. W. Lohmann and D. Mendlovic, "Temporal perfect-shuffle optical processor," *Opt. Lett.*, vol. 17, no. 11, pp. 822–824, June 1992.

[7] M. J. Erro, M. A. G. Laso, D. Benito, M. J. Garde, and M. A. Muriel, "A novel electrically tunable dispersion compensation system," *IEEE J. Select. Topics Quantum Electron*, vol. 5, pp. 1332–1338, Sept./Oct. 1999.

[8] A. W. Lohmann and D. Mendlovic, "Temporal filtering with time lenses," *Appl. Opt.*, vol. 31, no. 29, pp. 6212–6219, Oct. 1992.

[9] J. R. Klauder, A. C. Price, S. Darlington, and W. J. Albersheim, "The theory and design of chirp radars," *Bell Syst. Tech. J.*, vol. 39, pp. 745–808, 1960.

[10] T. Jannson, "Real-time Fourier transformation in dispersive optical fibers," *Opt. Lett.*, vol. 8, no. 4, pp. 232–234, Apr. 1983.

[11] M. A. Jack, P. M. Grant, and J. H. Collins, "The theory, design, and applications of surface acoustic wave Fourier-transform processors," *Proc. IEEE*, vol. 68, pp. 450–468, Apr. 1980.

[12] H. R. Fetterman, P. E. Tannenwald, C. D. Parker, J. Melngailis, R. C. Williamson, P. Woskoboinikow, H. C. Praddaude, and W. J. Mulligan, "Real-time spectral analysis of far-infrared laser pulses using a SAW dispersive delay line," *Appl. Phys. Lett.*, vol. 34, no. 2, pp. 123–125, Jan. 1979.

[13] Y. C. Tong, L. Y. Chan, and H. K. Tsang, "Fiber dispersion or pulse spectrum measurement using a sampling oscilloscope," *Electron. Lett.*, vol. 33, no. 11, pp. 983–985, May 1997.

[14] M. A. Muriel, J. Azaña, and A. Carballar, "Real-time Fourier transformer based on fiber gratings," *Opt. Lett.*, vol. 24, no. 1, pp. 1–3, Jan. 1999.

[15] H. Hakimi, F. Hakimi, K. L. Hall, and K. A. Rauschenbach, "A new wide-band pulse-restoration technique for digital fiber-optic communication systems using temporal gratings," *IEEE Photon. Technol. Lett.*, vol. 11, pp. 1048–1050, Aug. 1999.

[16] T. Lopetegi, M. A. G. Laso, J. Hernández, M. Bacaicoa, D. Benito, M. J. Garde, M. Sorolla, and M. Guglielmi, "New microstrip 'wiggly-line' filters with spurious passband suppression," *IEEE Trans. Microwave Theory Tech.*, vol. 49, pp. 1593–1598, Sept. 2001.

[17] M. A. G. Laso, T. Lopetegi, M. J. Erro, D. Benito, M. J. Garde, and M. Sorolla, "Multiple-frequency-tuned photonic bandgap microstrip structures," *IEEE Microwave Guided Wave Lett.*, vol. 10, pp. 220–222, June 2000.

[18] T. Lopetegi, M. A. G. Laso, M. J. Erro, D. Benito, M. J. Garde, F. Falcone, and M. Sorolla, "Novel photonic bandgap microstrip structures using network topology," *Microwave Opt. Technol. Lett.*, vol. 25, no. 1, pp. 33–36, Apr. 2000.

[19] M. A. G. Laso, T. Lopetegi, M. J. Erro, D. Benito, M. J. Garde, M. A. Muriel, M. Sorolla, and M. Guglielmi, "Chirped delay lines in microstrip technology," *IEEE Microwave Wireless Comp. Lett.*, vol. 11, pp. 486–488, Dec. 2001.

[20] A. M. Khilla, "Optimum continuous microstrip tapers are amendable to computer aided design," *Microwave J.*, pp. 221–224, May 1983.

[21] T. Lopetegi, M. A. G. Laso, M. J. Erro, M. Sorolla, and M. Thumm, "Analysis and design of periodic structures for microstrip lines by using the coupled-mode theory," *IEEE Microwave Wireless Comp. Lett.*, vol. 12, pp. 167–80, Nov. 2002.

[22] M. A. G. Laso, M. J. Erro, T. Lopetegi, D. Benito, M. J. Garde, and M. Sorolla, "Optimization of tapered Bragg reflectors in microstrip technology," *Int. J. Infrared Millim. Waves*, vol. 21, no. 2, pp. 231–245, Feb. 2000.

[23] D. M. Pozar, *Microwave Engineering*, 2nd ed. Reading, MA: Addison-Wesley, 1998.

[24] F. Sporleder and H.-G. Unger, *Waveguide Tapers, Transitions and Couplers*. London, U.K.: Peregrinus, 1979.

[25] E. Yamashita, K. Atsuki, and T. Ueda, "An approximate dispersion formula of microstrip lines for computer-aided design of microwave integrated circuits," *IEEE Trans. Microwave Theory Tech.*, vol. MTT-27, pp. 1036–1038, Dec. 1979.

[26] T. C. Edwards and M. B. Steer, *Foundations of Interconnect and Microstrip Design*, 3rd ed. Chichester, U.K.: Wiley, 2000.

[27] M. Anaya, J. A. Marcotegui, T. Lopetegi, M. A. G. Laso, and M. Sorolla, "Analysis of new periodic structures in microstrip by FDTD," presented at the Eur. Congr. on Computational Methods in Appl. Sciences and Eng., Barcelona, Spain, Sept. 2000.

[28] V. Radisic, Y. Qian, R. Coccioli, and T. Itoh, "Novel 2-D photonic bandgap structure for microstrip lines," *IEEE Microwave Guided Wave Lett.*, vol. 8, pp. 69–71, Feb. 1998.

[29] O. W. Otto, "Real time Fourier transform with a surface wave convolver," *Electron. Lett.*, vol. 8, no. 25, pp. 623–625, Dec. 1972.

[30] E. G. S. Paige, "Dispersive filters: their design and application to pulse compression and temporal transformations," in *IEE Conf.*, vol. 109, 1973, Pub. 61, pp. 167–180.

[31] C. C. W. Ruppel, L. Reindl, and R. Weigel, "SAW devices and their wireless communications applications," *IEEE Microwave Mag.*, pp. 65–71, June 2002.

[32] W. G. Lyons, D. R. Arsenault, A. C. Anderson, T. C. L. G. Sollner, P. G. Murphy, M. M. Seaver, R. R. Boisvert, R. L. Slattery, and R. W. Ralston, "High temperature superconductive wideband compressive receivers," *IEEE Trans. Microwave Theory Tech.*, vol. 44, pp. 1258–1277, July 1996.

[33] R. S. Withers, A. C. Anderson, P. V. Wright, and S. A. Reible, "Superconductive tapped delay lines for microwave analog signal processing," *IEEE Trans. Magn.*, vol. MAG-19, pp. 480–484, May 1983.

[34] F. Huang, "Quasitransversal synthesis of microwave chirped filters," *Electron. Lett.*, vol. 28, no. 11, pp. 1062–1064, May 1992.

[35] ——, "Low loss quasitransversal microwave filters with specified amplitude and phase characteristics," *Proc. Inst. Elect Eng.*, pt. H, vol. 140, no. 6, pp. 433–440, Dec. 1993.

[36] ——, "Possible design procedure for low-loss 180° reflecting arrays in SAW devices," *IEEE Trans. Ultrason., Ferroelect., Freq. Contr.*, vol. 35, pp. 57–60, Jan. 1988.

[37] ——, "Addendum to possible desing procedure for low-loss 180° reflecting arrays in SAW devices," *IEEE Trans. Ultrason., Ferroelect., Freq. Contr.*, vol. 36, pp. 385–386, May 1989.

[38] R. Guenther, *Modern Optics*. New York: Wiley, 1990.

[39] S. Qian and D. Chen, *Joint Time-Frequency Analysis: Methods and Applications*. Englewood Cliffs, NJ: Prentice-Hall, 1996.

[40] L. Cohen, *Time-Frequency Analysis*. Englewood Cliffs, NJ: Prentice-Hall, 1995.

[41] M. A. G. Laso, D. Benito, T. Lopetegi, M. J. Erro, M. J. Garde, M. A. Muriel, M. Sorolla, and M. Guglielmi, "Microstrip chirped delay lines based on photonic band-gap structures," in *Proc. 32nd Eur. Microwave Conf.*, vol. I, Milan, Italy, Sept. 2002, pp. 389–392.

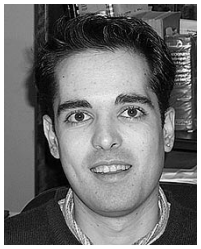

Miguel A. G. Laso (S'99–M'03) was born in Pamplona, Spain, in 1973. He received the M.Sc. and Ph.D. degrees in telecommunication engineering from the Public University of Navarre, Navarre, Spain, in 1997 and 2002, respectively.

From 1998 to 2002, he was awarded a grant from the Spanish Ministry of Education to support the research in his doctoral thesis at the Electrical and Electronic Engineering Department, Public University of Navarre, where he has been an Assistant Professor since 2001. His interests include electromagnetic crystals in planar microwave and millimeter-wave technologies and structures of photonic crystal in optical fibers. He has been involved in several projects funded by the Spanish Government and the European Union. Currently, he is with the Payload System Division, European Space Research and Technology Center (ESTEC), European Space Agency (ESA), Noordwijk, The Netherlands, where he is performing post-doctoral work on satellite applications of electromagnetic crystals in the microwave range.

Txema Lopetegi (S'99–M'03) was born in Pamplona, Spain, in 1973. He received the M.Sc. and Ph.D. degrees in telecommunication engineering from the Public University of Navarre, Navarre, Spain, in 1997 and 2002, respectively.

Since 1997, he has been with the Electrical and Electronic Engineering Department, Public University of Navarre, as an Academic Associate from 1997 to 1999, and as an Assistant Professor since 2000. In 1999 and 2000, he was awarded a grant from the Spanish Ministry of Education to support the research in his doctoral thesis. His research interests include passive devices and electromagnetic crystals in planar microwave and millimeter-wave technologies, with special concern to the microstrip technology. He has been involved in several projects funded by the Spanish Government and the European Union. Currently, he is with the Payload System Division, European Space Research and Technology Center (ESTEC), European Space Agency (ESA), Noordwijk, The Netherlands, where he is performing post-doctoral work on satellite applications of electromagnetic crystals in the microwave range.

María J. Erro (S'98–A'01) was born in Pamplona, Spain, in 1972. She received the M.Sc. and Ph.D. degrees from the Public University of Navarre, Navarre, Spain, in 1996 and 2001, respectively.

Since 1999, she is an Assistant Professor at the Electrical and Electronic Engineering Department, Public University of Navarre. From 2001 to 2002, she was also with the Polytechnic University of Valencia, Valencia, Spain, where she has performed her post-doctoral work in gratings in optical fibers. Her main interests include fiber Bragg gratings for dispersion compensation and electromagnetic crystals. She has been involved in several projects funded by the Spanish Government and the European Union.

Dr. Erro received the award for the Best Doctoral Thesis from the Spanish College of Telecommunication Engineers in 2002.

David Benito was born in Huesca, Spain, in 1965. He received the M.Sc. and Ph.D. degrees from the Polytechnic University of Madrid, Madrid, Spain, in 1992 and 1999, respectively.

Since 1992, he has been an Associate Professor with the Electrical and Electronic Engineering Department, Public University of Navarre, Navarre, Spain, where he currently leads the research activities on microwave photonics. His main interests include electrooptic modulators, fiber Bragg gratings, electromagnetic crystals, and nonlinear effects in optical fibers and their applications to radio-fiber systems. He has also been a member of several research projects supported by the Spanish Government and the European Union.

Dr. Benito received the award for the Best Doctoral Thesis from the Spanish College of Telecommunication Engineers in 2000.

María J. Garde was born in Pamplona, Spain, in 1964. She received the M.Sc. and Ph.D. degrees from the Complutense University of Madrid, Madrid, Spain, in 1987 and 1992, respectively.

Since 1992, she has been an Associate Professor with the Electrical and Electronic Engineering Department, Public University of Navarre, Navarre, Spain. Her main research interests include acoustooptical modulators, fiber Bragg gratings, and electromagnetic crystals. She has also been a member of several research projects supported by the Spanish Government and the European Union. She has supervised several doctoral theses in microwave photonics and optical fiber technology with the Public University of Navarre.

Miguel A. Muriel (M'84–SM'98) was born in Burgos, Spain, in 1955. He received the M.Sc. and Ph.D. degrees in telecommunication engineering from the Polytechnic University of Madrid, Madrid, Spain, in 1978 and 1980, respectively.

Since 1979, he has been with the Polytechnic University of Madrid, first as an an Assistant Professor (1980–1983) and an Associate Professor (1983–1989), and, since 1989, as a Full Professor. He has authored or coauthored numerous international papers and conference contributions in the fields of liquid crystals, optical bistability, optical chaos, pulse propagation in fibers, optical signal processing, linear and nonlinear resonators, fiber-optics sensors, fiber Bragg gratings, and time–frequency analysis. He has led ten research projects, some of them with Spanish and European industries, and he has acted as technical reviewer for several journals in the field of optoelectronics and optical communications. He has taught courses on optical electronics, optical communications, Fourier optics, electrooptical devices, and lasers. His professional interests cover fiber gratings, time–frequency representations, space–time duality, and, in general, signal processing applied to photonics and optical communications. He was Head of the Photonic Technology Department, Polytechnic University of Madrid, from September 1989 to October 1997.

Prof. Muriel is a member of the Optical Society of America. He received three awards for the Best Doctoral Thesis from the Menéndez y Pelayo University, Polytechnic University of Madrid, and the College of Telecommunication Engineers in Spain. He also received the Junior Research Award of the Polytechnic University of Madrid, Spain, in 1989, and the Senior Research Award of the same university in 1998.

Mario Sorolla (S'82–M'83–SM'01) was born in Vinaròs, Spain, in 1958. He received the M.Sc. degree from the Polytechnic University of Catalonia, Catalonia, Spain, in 1984, and the Ph.D. degree from the Polytechnic University of Madrid, Madrid, Spain, in 1991, both in telecommunication engineering.

He designed very high-power millimeter waveguides for plasma heating for the Euratom-Ciemat Spanish Nuclear Fusion Experiment from 1986 to 1990 and he was an Invited Scientist from 1987 to 1988 with the Institute of Plasma Research, Stuttgart University, Stuttgart, Germany. He has worked in microwave integrated circuits and monolithic microwave integrated circuits for satellite communications for the companies Tagra and Mier Communications in Spain. He has been an Assistant Professor with the Polytechnic University of Catalonia, Vilanova i la Geltrú, Spain, from 1984 to 1986, and with the Ramon Llull University, Barcelona, Spain, from 1991 to 1993. From 1993 to 2002, he was an Associate Professor with the Public University of Navarre, Navarre, Spain, where he is currently a Full Professor in the Electrical and Electronic Engineering Department. His research interests range from high-power millimeter waveguide components and antennas to coupled-wave theory and applications of electromagnetic crystals to microwave circuits and antennas.

Marco Guglielmi (M'78–SM'97) was born in Rome, Italy, in 1954. He received the Laurea degree in ingegneria elettronica from the University of Rome "La Sapienza," Rome, Italy, in 1979, the M.Sc. degree in electrical engineering from the University of Bridgeport, Bridgeport, CT, in 1982, and the Ph.D. degree in electrophysics from the Polytechnic University of Brooklyn, Brooklyn, NY, in 1986.

In 1980, he attended the Scuola di Specializzazione in Elettromagnetismo Applicato, University of Rome "La Sapienza." From 1984 to 1986, he was an Academic Associate with the Polytechnic University of Brooklyn, and an Assistant Professor with the same institution from 1986 to 1988. From 1988 to 1989, he was an Assistant Professor with the New Jersey Institute of Technology, Newark, NJ. In 1989, he joined the RF System Division, European Space Research and Technology Center (ESTEC), European Space Agency (ESA), Noordwijk, The Netherlands, where he was involved in the development of passive microwave components for space applications. His professional interests include the areas of solid-state devices and circuits, periodic structures, phased arrays and millimeter-wave leaky-wave antennas, network representations of waveguide discontinuities and microwave filtering structures. Currently, he is Head of the Technology Strategy Section, Technology Programs Department, ESTEC-ESA.

Dr. Guglielmi was the recipient of a 1981 Fulbright Scholarship and a Halsey International Scholarship Program (HISP) Scholarship from the University of Bridgeport.